https://doi.org/10.5194/essd-2026-614
Preprint. Discussion started: 2 September 2026

Open Access Earth System Science Data Discussions

A FAIR annotated set of 60k+ in situ zooplankton images from the Greater North Sea and Greenland

Pieter D. L. Hovenkamp[1, 4], Lodewijk van Walraven[2], Daan Temmerman[3], A. Frank van der Stappen[4, 5], and Dick van Oevelen[1]

[1]Department of Estuarine and Delta Systems, NIOZ Royal Netherlands Institute for Sea Research, Yerseke, The Netherlands. E-mail: pieter.hovenkamp@nioz.nl
[2]Hydrobiological Laboratory, Rijkswaterstaat, Lelystad, the Netherlands
[3]Department of Oceanic Systems, NIOZ Royal Netherlands Institute for Sea Research, Texel, The Netherlands
[4]Department of Information and Computing Sciences, Utrecht University, Utrecht, The Netherlands
[5]University College Roosevelt, Middelburg, The Netherlands

Correspondence: Pieter D. L. Hovenkamp (pieter.hovenkamp@nioz.nl)

Abstract. The North Sea is a productive shelf sea with a wide variety of hydrographic and biological conditions. It is subject to high anthropogenic pressures, including climate change, terrestrial nutrient loading, and the development of offshore wind farms, and the associated environmental changes have major consequences for zooplankton abundance and community composition. In situ imaging provides new opportunities to monitor meso- and macrozooplankton, as it enables sampling at meter-scale resolution and improved assessments of fragile gelatinous taxa. The vast amounts of data that can be collected with in situ imaging necessitate the use of automated data processing pipelines. However, developing these requires a substantial amount of expert-annotated data. In this paper, we share a large annotated set of plankton and particle images from an in situ shadowgraph imager (ISIIS-DPI, 46,331 images) and the Continuous Particle Imaging and Classification Sensor (CPICS, 14,496 images) among, respectively, 64 and 42 taxonomic and trait-based classes that were collected in the Greater North Sea and complemented with data from Greenland. Based on the geographical coverage, size distribution, and environmental data collected simultaneously with the images, we show that this set is taxonomically representative of the Greater North Sea. In addition, we trained Convolutional Neural Network classifiers, one for the ISIIS-DPI and one for the CPICS, and both achieved an F1-score of 80.1%, showing that these classifiers can be reliably used on newly collected ISIIS-DPI and CPICS data in this region. All annotated images, as well as location and environmental data, are shared publicly (10.5281/zenodo.21737141, Hovenkamp et al., 2026c) following a flexible taxonomic classification scheme to ensure flexible use and inter-operability with similar (future) sets. The annotated data and classifiers that we present should greatly facilitate zooplankton studies employing in situ imaging in the Greater North Sea. This improves our ability to assess how zooplankton communities are likely to respond to the ongoing anthropogenic pressure on the North Sea and addresses a critical knowledge need.

1 Introduction

The North Sea is a productive continental shelf sea that is under high anthropogenic stress (Emeis et al., 2015; McQuatters-Gollop et al., 2022). The sea surface temperature in the North Sea has increased rapidly compared to the global average

https://doi.org/10.5194/essd-2026-614
Preprint. Discussion started: 2 September 2026

Open Access Earth System Science Data Discussions

(Simpson et al., 2011) with roughly 0.2 to 0.4 °C per decade (Dye et al., 2013) and is projected to continue warming throughout the century (Dye et al., 2013; Quante and Colijn, 2016). Changes in terrestrial nutrient loading have affected pelagic ecosystems (Capuzzo et al., 2018; Desmit et al., 2020), which may additionally be impacted by the recent upscaling of offshore wind energy (Floeter et al., 2017; Isaksson et al., 2025; Zampollo et al., 2025). Zooplankton is highly sensitive to environmental conditions and climate change (Williams et al., 1994; Taylor et al., 2002; Drinkwater et al., 2003; Richardson, 2008), and forms a vital link in marine pelagic ecosystems, being the link between primary production and higher trophic levels. Moreover, zooplankton plays an important role in the global carbon cycle (Steinberg and Landry, 2017; Rohr et al., 2023). As such, zooplankton was used in several quality indicators in the latest OSPAR's quality status report (Holland et al., 2023), and therefore continued and novel monitoring of zooplankton dynamics is critically needed.

The Greater North Sea has a wide variety of hydrographic and ecological zones: southern regions are vertically mixed throughout the year, whereas northern regions are seasonally or permanently stratified, and transitional zones between the two exist (Van Leeuwen et al., 2015). In addition, differences exist between regions that are mostly influenced by Atlantic inflow, inflow from the Channel or dominated by river outflow (Otto et al., 1990; Enserink et al., 2019). As such, in recent OSPAR assessments the Greater North Sea (OSPAR region II) was divided into 29 distinct hydrographic zones, depending on physical, chemical, and biological conditions (Enserink et al., 2019). The wide variety of hydrographic zones reflects that biological data from a single location or depth are not necessarily representative of the whole region. For example, long-term changes in phytoplankton primary production were observed to vary between hydrographic regions (Capuzzo et al., 2018). This drives the need for increased, depth-resolved sampling efforts that better cover the Greater North Sea.

In situ imaging provides new opportunities for zooplankton sampling, overcoming some of the limitations of traditional sampling with nets or the Continuous Plankton Recorder Continuous Plankton Recorder (CPR, Batten et al., 2003). Gelatinous groups can be sampled more accurately (Remsen et al., 2004; Luo et al., 2014), and the meter-scale resolution of in situ imaging (Gallager, 2016; Cowen and Guigand, 2008) allows studying fine-scale vertical distributions and habitat preferences of meso- and macrozooplankton (e.g. Luo et al., 2014; Greer et al., 2015; Schmid et al., 2023). Moreover, planktonic size spectra can be constructed relatively easily from images (Grosjean et al., 2004; Hovenkamp et al., 2026a). From size spectra, the trophic transfer efficiency can be estimated (Zhou, 2006) through a single and inter-comparable index, allowing for large-scale analysis of planktonic food webs (e.g. Atkinson et al., 2021, 2024). With in situ imaging, a vast number of plankton images are collected (up to millions per study, Schmid et al., 2020; Hovenkamp et al., 2026a). This drives the need for automated data processing pipelines for taxonomic classification (Irisson et al., 2022), which have been successfully applied in various recent studies (e.g. Luo et al., 2018; Schmid et al., 2020). With the combination of in situ imaging and automated processing of the data, sampling efforts can be increased with limited additional costs, and this enables a potentially vast increase in the spatial and temporal scale of zooplankton monitoring.

For successful application of a fully automated classification pipeline, a manually annotated set of images is required for all taxonomic groups of interest that can be expected (e.g. Orenstein et al., 2022). However, obtaining a representative annotated set comes with challenges. Manual annotation of images is time-consuming, especially when large amounts of marine snow, often present in shelf seas, can reduce the number of living images to as little 1% of all data (Forest et al., 2012). In addition,

https://doi.org/10.5194/essd-2026-614
Preprint. Discussion started: 2 September 2026

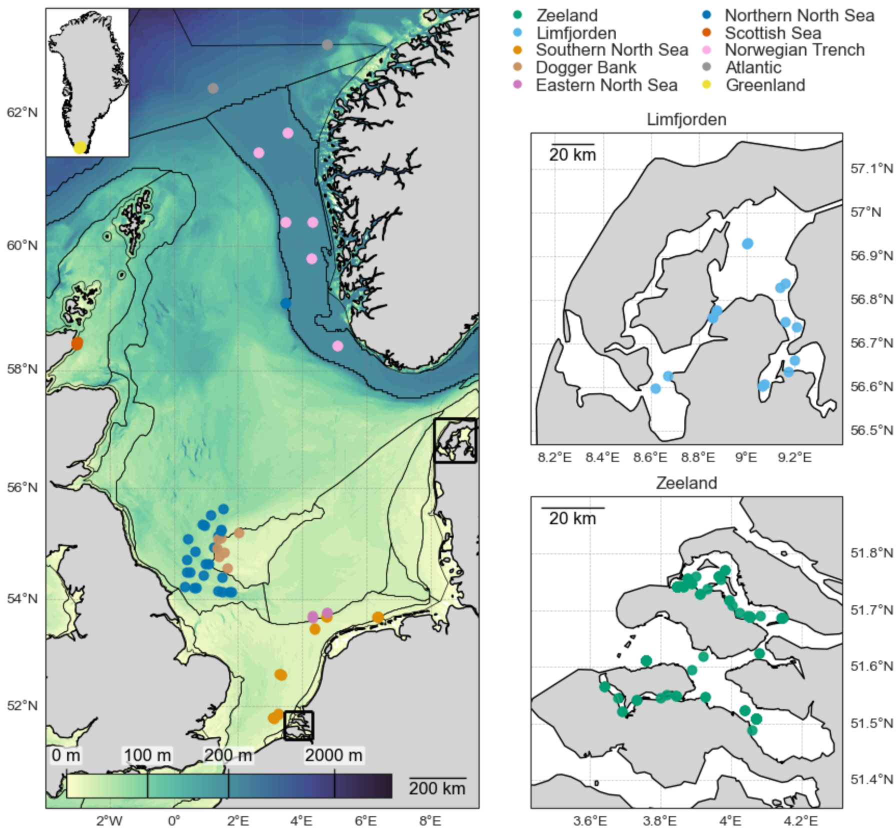

Figure 1. Map of the study region with markers for all transects that were sampled with the ISIIS-DPI and CPICS that were included in the annotated set. Solid lines denote the pelagic OSPAR Common Procedure Assessment Units for the Greater North Sea (Enserink et al., 2019), and sampling sites are colour-coded accordingly, with additional regions defined for Zeeland (The Netherlands), Limfjorden (Denmark) and Greenland.

with the variety of ecological zones within the Greater North Sea, using a learning set from one area to classify data from another area carries the risk of missing organisms that are characteristic of the study region. This underlines the need for a learning set with a broad geographical coverage. Finally, useful exchange of annotated data between research groups, if available, is commonly inhibited due to a lack of provided metadata (e.g., sampling location) and a common classification scheme (Horton et al., 2021; Irisson et al., 2022).

In this paper, we present a large, annotated set of over 60000 images from two in situ imaging instruments: the In Situ Ichthyoplankton Imaging System Deep-focus Particle Imager (ISIIS-DPI) and the Continuous Particle Imaging and Classification Sensor (CPICS). By combining images from various regions representing different ecological zones, we create a set that is representative of the meso- and macrozooplankton communities in the Greater North Sea. Taxonomic information and metadata of all images are stored in line with the framework presented by (Van Walraven et al., 2026, under review), so that

Findable, Accessible, Interoperable, and Reusable (FAIR) usage of the set is guaranteed. This enables users to create subsets of the annotated data that are relevant for their use-case. In addition, we present a Convolutional Neural Network (CNN) classifier that is trained on the annotated set per instrument and can be used in an automated classification pipeline. With the published data sets and classifiers, we aim to facilitate zooplankton monitoring efforts and studies that use in situ imaging within the Greater North Sea.

2 Methods

2.1 Study regions

Data were collected in the Greater North Sea region between February 2021 and June 2024. The Greater North Sea dataset was further complemented with annotated ISIIS-DPI data (11829 images) from a research campaign in southwest Greenland in 2023 (Hovenkamp et al., unpublished). Although the focus of the present study was the Greater North Sea, data from Greenland were added due to the observed similarity of taxonomic classes between Greenland and some North Sea regions and the associated potential to improve the classification of North Sea plankton by increasing the size of the annotated set. An overview of the study sites and research cruises is presented in Figure 1 and Table 1, respectively.

We grouped the annotated data following the pelagic OSPAR Common Procedure Assessment Units for the Greater North Sea, which were developed by Enserink et al. (2019) and used in the 2023 OSPAR Quality Status Report to assess, among others, phyto- and zooplankton communities (Holland et al., 2023). Additional regions were defined for Greenland and the inshore marine sampling sites in the Dutch Zeeland delta (hereafter 'Zeeland') and the Danish Limfjorden, as these are not within the regional assessment units. For two cruises (Northern North Sea, 2023, and Norwegian Trench, 2024, Table 1), location data that were just outside the defined regional assessment units were assigned to the nearest unit ('Scottish Sea' and 'Atlantic', respectively, Figure 1).

The presented manually annotated data are a subset of all images that were collected in these campaigns. The ecological analysis of the complete data sets is presented in separate manuscripts, e.g., for the North Sea Doggersbank (Hovenkamp et al., 2026a), southern Greenlandic fjords (Hovenkamp et al., unpublished) and for the Norwegian Trench and Norwegian Sea (Temmerman et al. in preparation).

2.2 Imaging instruments

The ISIIS-DPI (Bellamare, Cowen and Guigand, 2008; Greer et al., 2025) is an in situ shadowgraph imaging system, of which we used an area-scan configuration with a field of view of 8.83 cm (5328 pixels) $\times$ 7.64 cm (4608 pixels). The pixel resolution and maximum frame rate were, respectively, 17 µm (5328 $\times$ 4608 pixels) and 5 Hz from June 2022 to August 2023, and 38 µm (2448 $\times$ 2048 pixels) and 20 Hz from September 2023 onwards. In September 2023, the internal camera was replaced. This was necessary to reduce the data flow between the camera and storage device and did not lead to a visible reduction in the image quality or amount of taxonomic detail. The adjustable depth of field varied between 10 cm (in turbid conditions) and 35 cm (in

https://doi.org/10.5194/essd-2026-614
Preprint. Discussion started: 2 September 2026

Open Access Earth System Science Data Discussions

Sampling area	Period	Reference	Number of deployments		Total deployment duration (hour)		Number of collected images	
			CPICS	ISIIS-DPI	CPICS	ISIIS-DPI	CPICS	ISIIS-DPI (full-frames / ROIs)
Zeeland, The Netherlands	2021, 25/2-18/11	Van Oevelen et al. in prep.	156	-	212:50	-	3,321,824	-
North Sea Borkum Grounds	2021, 4/4		1	-	5:57	-	337,402	-
Belgian North Sea	2021, 6/5-7/5		5	-	8:17	-	183,334	-
Zeeland, The Netherlands	2022, 25/3-29/3		18	-	30:18	-	2,066,255	-
Zeeland, The Netherlands	2022, 20/6-23/6		15	15	11:37	11:37	232,299	174,123 / 51,266,178
Southern North Sea	2022, 28/6-30/6		3	3	37:36	37:36	282,094	198,232 / 12,855,0818
Southern North Sea	2022, 5/7-14/7		7	6	49:27	45:42	1,283,233	399,302 / 158,435,992
Zeeland, The Netherlands	2022, 23/9-29/9		17	16	44:56	42:08	1,034,119	525,864 / 104,925,792
North Sea Dogger Bank	2023, 17/6-25/6	Hovenkamp et al. (2026a)	22	10	18:44	40:34	133,841	247,044 / 72,481,113
Southwest Greenland	2023, 18/7-1/8	Hovenkamp et al., unpub.	11	10	27:03	25:16	150,656	385,981 / 23,445,230
Zeeland, The Netherlands	2023, 19/9-20/9		-	5	-	9:07	-	407,845 / 2,497,651
Northern North Sea	2023, 2/10-9/10		9	9	19:39	19:39	132,945	781,710 / 13,948,076
Southern North Sea	2024, 16/4-21/4		2	2	5:04	5:04	275,857	353,670 / 100,550,809
Norwegian Trench	2024, 28/4-16/6	Temmerman et al. in prep.	9	9	15:53	15:53	20,847	502,864 / 2,421,243
Limfjorden, Denmark	2024, 17/6-21/6		8	8	10:25	10:25	80,315	657,152 / 105,446,455

Table 1. Overview of the sampling campaigns of which data was used in this study. Coordinates of the sampling locations are available online per annotated image.

clear conditions), resulting in a sampling volume of 12 to 43 $\mathrm{m^3\,h^{-1}}$ (at 5 Hz) and 49 to 170 $\mathrm{m^3\,h^{-1}}$ (at 20 Hz). The ISIIS-DPI is able to sample plankton from (approximately) 500 µm up to several centimeters in length, a size range that includes large phytoplankton (e.g. Phaeocystis colonies, long-chained diatoms), large copepods, meroplankton, gelatinous zooplankton and ichthyoplankton. The ISIIS-DPI stores full-frame images that contain tens to hundreds of organisms and particles. Therefore, a post-processing segmentation procedure (following Hovenkamp et al., 2026a) was applied to extract individual Regions of Interest (ROIs, see Figure 2 for examples).

The CPICS-1000-e (referred to as CPICS hereafter, Gallager, 2016, Coastal Ocean Vision) is an *in situ* imaging system that collects dark-field colour images of plankton and particles of approximately 200 µm to 1.5 cm. We used a set-up with a 0.9$\times$ magnification lens, a pixel resolution of 4.54 µm, an image resolution of 2736 $\times$ 2192 pixels, and a factory-calibrated depth of view of 2 mm. This results in a field of view of 15 mm $\times$ 11 mm and a sampling volume of 0.33 mL per full-frame image. The frame rate of the system can theoretically reach 13 Hz, although in practice the maximum achievable frame rate was $\sim$ 8 Hz throughout our sampling campaigns, leading to a realized sampling volume of 9.5 $\mathrm{L\,h^{-1}}$. The CPICS uses an on-board segmentation procedure that detects and stores ROIs (Figure 3). A considerable amount of ROIs that we collected were too unsharp for taxonomical classification. Therefore, during post-processing we used Canny's edge detection algorithm (Canny, 1986, using $\sigma = 3$, and as low and high threshold, respectively, 10% and 20% of the maximum pixel intensity) to remove all unsharp ROIs, i.e., those that contained no detected edge pixels.

Depending on the campaign, either one or both the CPICS and ISIIS-DPI were mounted on a frame (Figure A1) along with a CTD (Conductivity Temperature Depth, RBRMaestro or Sea-Bird SBE9) with additional sensors for turbidity (Seapoint Tu or WET Labs ECO), dissolved oxygen concentration (RBRcoda T.ODO or SBE 43), and fluorescence (Turner Cyclops or Chelsea Aqua 3). This frame was towed from the aft of a vessel with a towing speed of 2 to 5 knots while undulating between the surface and sea floor (i.e. 'tow-yo'-ing), it or was undulated while the vessel was stationary (i.e. 'yo-yo'-ing). In some surveys, the imaging instruments were mounted on a video frame alongside a seafloor observing camera system, and this frame was slowly towed (0.5 to 1 knots) at 1 to 2 m above the seafloor. The deployment method depended on the research vessel, the oceanographic conditions, and the objectives of the study.

2.3 Annotation workflow

For the ISIIS-DPI set, 13,417 ROIs were annotated by Hovenkamp et al. (2026a) in a study on the North Sea Dogger Bank, and 11,829 ROIs (hereafter referred to as 'images') in a study in southwest Greenland (Hovenkamp et al., unpublished). In this paper, we significantly extended this annotated set to make it representative of the Greater North Sea by annotating a large additional set of images and extending the number of taxonomic classes.

Finding images of living plankton in large amounts of unlabeled data can be a needle-in-a-haystack problem as a result of the large fraction of non-living particles that is often present in shelf seas (Forest et al., 2012) and the strong imbalance in the natural abundances of taxonomic classes (Schröder et al., 2019; Eerola et al., 2024). Therefore, we applied the following procedure to annotate images. First, we applied the automated CNN classifier presented by Hovenkamp et al. (2026a) to a size-stratified subsample of at most 10 million collected ISIIS-DPI images of each campaign listed in Table 1, except for the

https://doi.org/10.5194/essd-2026-614
Preprint. Discussion started: 2 September 2026

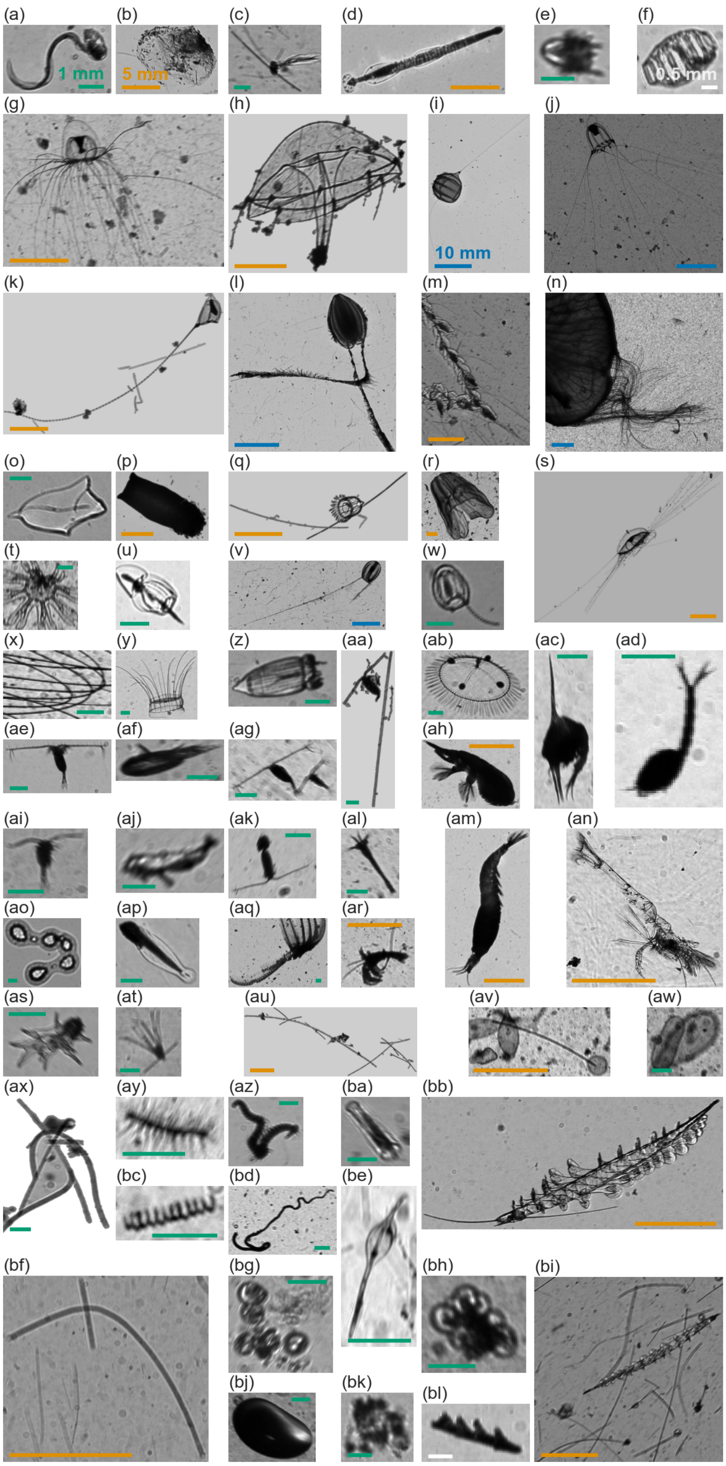

Figure 2. Regions of Interest (ROIs) of the ISIIS-DPI (caption continues on next page)

https://doi.org/10.5194/essd-2026-614
Preprint. Discussion started: 2 September 2026

for all classes in the annotated set. The size of ROIs is indicated by scalebars of the same colour: white is 0.5 mm (panel bl and f), green is 1 mm (panel a, c, e, o, t, u, w, x, y, z, aa, ab, ac, ad, ae, af, ag, ai, aj, ak, al, ao, ap, aq, as, at, aw, ax, ay, az, ba, bc, bd, be, bg, bh, bj and bk), orange is 5 mm (panel b, d, g, h, k, m, q, r, s, p, am, an, bb, bf, bi, au, av, ah and ar) and blue is 10 mm (panel n, j, i, l and v) true size. The corresponding class names are: **a)** Appendicularian, **b)** Appendicularian house empty, **c)** Diatom chain with appendicularian, **d)** Chaetognath, **e)** Ctenophore Tentaculata small, **f)** Thaliacea Doliolida, **g)** Cnidarian bell-shaped, **h)** Cnidarian Eirenida, **i)** Ctenophore *Dryodora glandiformis*, **j)** Cnidarian *Leuckartiara sp.*, **k)** Cnidarian *Corymorpha nutans*, **l)** Ctenophore *Mertensia ovum*, **m)** Cnidarian Siphonophore Physonect colony, **n)** Cnidarian Scyphozoa, **o)** Cnidarian Siphonophore Physonect zooid, **p)** Ctenophore *Beroe sp.*, **q)** Diatom chain with *Aglantha digitale*, **r)** Ctenophore Lobata, **s)** Cnidarian oblate, **t)** Cnidarian Scyphozoa ephyra, **u)** Cnidarian Siphonophore Calycophora, **v)** Ctenophore Cydippida, **w)** Cnidarian *Euphysa Aurata*, **x)** Tentacle, **y)** Cnidarian Narcomedusa, **z)** Cnidarian *A. digitale*, **aa)** Diatom chain with copepod, **ab)** Cnidarian *Obelia sp.*, **ac)** Crustacean Brachyura zoea, **ad)** Crustacean Cumacea, **ae)** *Calanus sp.* antennae extended, **af)** Copepod antennae folded, **ag)** Copepod multiple, **ah)** Crustacean Amphipod, **ai)** Copepod other antennae extended, **aj)** Copepod exuvium, **ak)** Copepod with eggs, **al)** Crustacea other small, **am)** Crustacea other large, **an)** Crustacean other exuvium, **ao)** Eggs unknown, **ap)** Fish larva, **aq)** Cirripedia moult, **ar)** Crustacean Megalopa, **as)** Echinoderm Asteroidea, **at)** Echinoderm pluteus, **au)** Diatom chain with particle, **av)** Diatom chain with Phaeocystis, **aw)** Phaeocystis, **ax)** Diatom chain region, **ay)** Diatom chain with setae, **az)** Polychaete other, **ba)** Polychaete with tube, **bb)** Polychaete *Tomopteris sp.*, **bc)** Diatom chain curled, **bd)** Worm unknown, **be)** *Noctiluca scintillans* with ingested diatom chain, **bf)** Diatom chain, **bg)** *N. scintillans*, **bh)** *N. scintillans* with detritus, **bi)** Diatom chain with *Tomopteris sp.*, **bj)** Bubble, **bk)** Non-living, **bl)** Polyp benthic fragment.

campaigns to the Dogger Bank and Greenland, as these were already annotated. Per predicted class, a subset of images with the highest and lowest classifier confidence was annotated from each campaign. Annotating low-confidence predictions is thought to be an efficient way of providing 'new information' to a classifier (Bochinski et al., 2019), and we experienced that images with a low-confidence prediction often contain unseen or rare organisms. By using size-stratified subsampling, it was ensured that all size classes are represented in the annotated set. Omitting this step would lead to a heavily under-representation of the larger size classes, given the exponential decrease of organism abundance with increasing size (Sheldon et al., 1972) and the fact that the images span a size range of roughly two orders of magnitude.

The CPICS set was based on a set of 8037 ROIs (hereafter 'images') collected and annotated by Van Oevelen et al. (in preparation) in Zeeland. Similar to the ISIIS-DPI set, this set was substantially expanded to a set that is representative for the Greater North Sea: A previous CNN classifier (Hovenkamp et al., 2026b) was applied to the CPICS images of all campaigns (Table 1), and we annotated a subset of images for each predicted class per campaign.

In addition to the taxonomic identifications of the images, several descriptive features were encountered during annotation of the ISIIS-DPI and CPICS sets. These attributes were annotated separately and are discussed in more detail in the Results section. The annotations of all ISIIS-DPI and CPICS images were validated by two observers (PH and LvW).

2.4 Data set structure

The annotations assigned to the images were structured following the flexible image classification scheme described by Van Walraven et al. (2026, under review). The core of this classification scheme is that the information of each image is

https://doi.org/10.5194/essd-2026-614
Preprint. Discussion started: 2 September 2026

Figure 3. Regions of Interest (ROIs) of all CPICS classes in the annotated set. The size of ROIs is indicated by scalebars of the same colour. green is 0.1 mm (panel t, ae and s), white is 0.2 mm (panel a, b, c, d, e, h, j, k, l, n, o, p, q, r, u, v, w, y, z, ab, af, ag, ah, ai, aj, al, am, an and ao), and blue is 0.5 mm (panel f, m, g, i, aa, ac, ap, ad, ak and x). The corresponding class names are: **a)** Appendicularian, **b)** Appendicularian house (part), **c)** Copepod calanoid, **d)** Copepod calanoid with eggs, **e)** Copepod nauplius, **f)** Cnidarian hydrozoan, **g)** Tentacle, **h)** Ascidian larva, **i)** Crustacean amphipoda, **j)** Copepod cyclopoid, **k)** Copepod exuvium, **l)** Copepod harpactacoid, **m)** Ctenophore, **n)** Diatom chain, **o)** Diatom Pleurosigma, **p)** *Noctiluca scintillans*, **q)** Copepod cyclopoid with eggs, **r)** Copepod harpactacoid with eggs, **s)** Trochophore, **t)** Ctenophore egg, **u)** Diatom centric, **v)** Crustacean decapod larva, **w)** Balanoid nauplius, **x)** Echinoderm Asteroidea, **y)** Flatworm, **z)** Echinoderm pluteus, **aa)** Crustacean caprella, **ab)** Gastropod veliger, **ac)** Balanoid exuvium, **ad)** Fish larva, **ae)** Crustacean cladocera, **af)** Cnidarian planula, **ag)** Polychaete larva. **ah)** Polychaete metatrochophore **ai)** Rotifer **aj)** Rotifer with eggs **ak)** Macroalgae fragment **al)** Gastropod egg **am)** Bivalve veliger **an)** Bubble **ao)** Detritus **ap)** Phaeocystis.

https://doi.org/10.5194/essd-2026-614
Preprint. Discussion started: 2 September 2026

stored in a database (see Table 2 for an example). This database contains taxonomic information on each image, as well as several additional attributes, holding information such as 'carrying eggs' or details on larval stages. The detailed taxonomic identifications are grouped into three larger categories: one for organisms, which are identified up to the highest taxonomic level we were able to achieve, one for particles that carry taxonomic information ('taxo particle'), such as barnacle moults and copepod exuvia, and one for particles that do not hold any taxonomic information ('non-taxo particle'). By adopting this scheme, we explicitly distinguish between the annotated set, being the set of images with all taxonomic and descriptive information, and a learning set, which is used to train a machine learning classifier. For a learning set, taxonomic groups or images from specific regions of the annotated set can be selected, omitted, or merged, depending on the application. Thus, by querying the database, a learning set instance can be easily generated that best suits the classification problem at hand.

The annotated sets were published on Zenodo (10.5281/zenodo.21737141, Hovenkamp et al., 2026c) via a zip-file containing all images, and an accompanying csv-file with per image: a unique identifier, the assigned label including the aphiaID from WoRMS (Ahyong et al., 2026), attributes, CTD data, date and time of collection, and geographical coordinates (Table 2). In case of future improvements of the annotated set, e.g. by further increasing the taxonomic resolution of labels or by adding new images, each previous version will be kept publicly available to ensure reproducibility of scientific output that is based on the current set.

2.5 Convolutional Neural Network training

To showcase the value of the annotated sets for automated image classifcation, a CNN called 'EfficientNetV2S' (Tan and Le, 2021) was trained based on the annotated sets, one for the ISIIS-DPI and one for the CPICS. The learning sets were generated from all combinations of taxa and attributes that contained at least 20 images. For the ISIIS-DPI and CPICS, classes with more than 100 images were shown to give a reliably high class-specific performance with a CNN classifier (Hovenkamp et al., 2026b). Below this number, the performance may be lower depending on, for example, morphological resemblance with other classes. Here, we nevertheless included classes with 20 to 100 images in the learning set in order to showcase the capacity of the classifier on a large number of classes, including classes with few data, but we note that the most substantial improvements to the classifiers could be made by expanding these rare classes within our annotated sets.

The procedure we applied to train the CNNs involved transfer learning using ImageNet weights (Deng et al., 2009), balanced class weights, and hyperparameter tuning of the learning rate and optimizer's weight decay, and is further described in Hovenkamp et al. (2026b). In addition, a hierarchical loss function was utilized to reduce false predictions of (numerically dominant) non-living classes into living classes (in line with Bertinetto et al., 2020; Hovenkamp et al., 2026a).

The performance of the classifiers was evaluated on the test set and is reported in terms of per-class precision ($\frac{\mathrm{TP}}{\mathrm{TP+FP}}$ with TP and FP respectively the number of true and false positives), recall ($\frac{\mathrm{TP}}{\mathrm{TP+FN}}$ with FN the number of false negatives) and F1-score ($2 \times \frac{\mathrm{precision} \times \mathrm{recall}}{\mathrm{precision+recall}}$). Precision quantifies the number of correct predictions in a class ('purity'), recall how many true labels of a class are predicted as that class ('completeness') and F1-score (per-class) is the harmonic mean of precision and recall.

https://doi.org/10.5194/essd-2026-614
Preprint. Discussion started: 2 September 2026

Image identifier	Name	Taxonomic information		Attribute			Metadata				
		Group	aphiaID	Life stage	Carrying eggs	...	Region	Longitude	Latitude	Salinity	...
ISIIS-DPI_*datetime*	Appendicularian	Organism	146421				Northern North Sea	1.221	54.951	34.60	
ISIIS-DPI_*datetime*	Copepod with eggs	Organism	1080	Adult	Yes		Southern North Sea	3.081	51.793	33.97	
ISIIS-DPI_*datetime*	Copepod exuvium	Taxo particle	1080				Norwegian Trench	2.633	61.417	32.95	
CPICS_*datetime*	Copepod calanoid	Organism	1100		No		Dogger Bank	2.008	55.216	34.75	
CPICS_*datetime*	Echinoderm	Organism	1806	Pluteus			Southern North Sea	3.084	51.791	33.96	
CPICS_*datetime*	Detritus	Non-taxo particle					Zeeland	3.890	51.595	30.48	

Table 2. Example of the csv-database containing the annotations and metadata of the images. Empty cells under attributes indicate that an attribute was not checked for. The adopted database structure was based on Van Walraven et al. (2026, under review).

https://doi.org/10.5194/essd-2026-614
Preprint. Discussion started: 2 September 2026

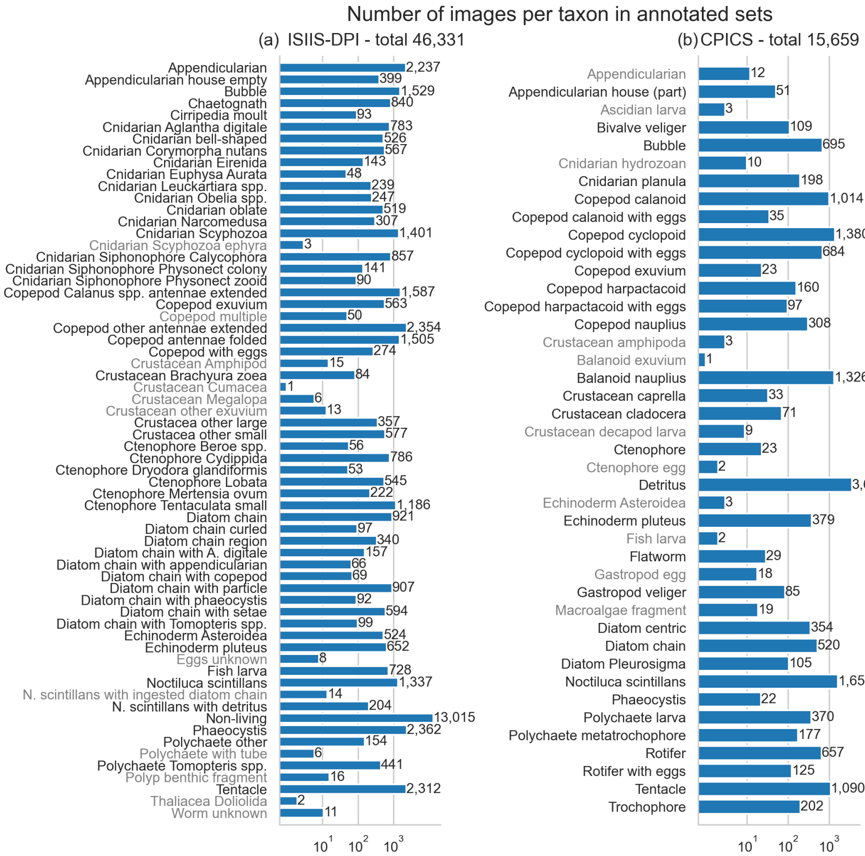

Figure 4. The assigned labels in the annotated sets of the ISIIS-DPI (a) and CPICS (b). Labels that were not included as a class in the learning set of the classifiers are displayed in gray.

To increase the reported precision of both classifiers, probability filtering (Faillettaz et al., 2016; Luo et al., 2018) was applied by determining class-specific probability thresholds on the validation set. Specifically, for each taxonomic class the threshold was determined such that i) the precision with respect to false predictions of the ground truth groups ‘non-living’ or ‘detritus’ and ‘bubble’ was greater than 99%, and ii) the precision with respect to false prediction from other taxonomic classes was greater than 80%. For the non-taxonomic classes (‘non-living’ or ‘detritus’ and ‘bubble’), a default threshold of 0.3 was used.

https://doi.org/10.5194/essd-2026-614
Preprint. Discussion started: 2 September 2026

3 Results

3.1 Description of annotated set

3.1.1 Taxonomic composition

For the ISIIS-DPI, a total of 46,331 images was annotated among 64 classes (Figure 4a), of which examples are shown in Figure 2. Of these, 28,391 images were in 56 living classes, 3396 in 6 taxonomic non-living classes (‘Appendicularian house empty’, ‘Cirripedia moult’, ‘Copepod exuvium’, ‘Crustacean other exuvium’, ‘polyp benthic fragment’ and ‘tentacle’) and 14,544 in the remaining non-living classes (‘non-living’ and ‘bubble’). In addition to the taxonomic identifications that were assigned, attributes were assigned to copepods with antennae extended and antennae folded, as these postures were suggested to reflect behavioural differences (Vilgrain et al., 2021). Also, a separate attribute was assigned to copepods if they were carrying eggs. Given the high density of diatom chains in certain regions (as described by Hovenkamp et al., 2026a), certain taxa were commonly observed to overlap with a diatom chain within a single image, and for these images an additional attribute ‘with diatom chain’ was assigned. For all combinations of assigned taxa and attributes, 41 of the ISIIS-DPI classes contain more than 100 images, and 11 classes contain less than 20 images.

A total of 15,659 CPICS images was annotated among 42 classes (Figure 3, and examples in Figure 4b). The annotated images were distributed among 36 living classes (11,265 images), 4 taxonomic non-living classes (‘Appendicularian house part’, ’Balanoid exuvium’, ‘Copepod exuvium’ and ‘Macroalgae fragment’, 94 images) and two non-living classes ‘detritus’ and ’bubble’ (4300 images). Attributes for egg-carrying individuals were annotated for the various copepod orders and for rotifers. Of all taxa and attributes, 11 of the CPICS classes contain fewer than 20 images, whereas 21 classes contain more than 100 images.

3.1.2 Regional coverage of annotated set

The origin of the annotated images is shown per taxonomic class in Figure 5. Although the regional distribution does not necessarily reflect true taxa abundances in the different regions, several species predominantly originate from a single region. For example, *Corymorpha nutans* in the ISIIS-DPI set all originated from the Northern North Sea, Narcomedusae from the Scottish Sea and Siphonophore zoids from the Norwegian Trench. This indicates the importance of basin-wide sampling for constructing a taxonomically representative annotated set.

In the CPICS set, several classes mainly originate from Zeeland. This is merely a consequence of our annotation effort. We started with an annotated set from Zeeland and expanded this set by focusing on the classes with few images and on taxonomic groups that had not been included yet. The size spectra of the annotated images (Figure 6) plotted on logarithmic axes roughly follow a negative linear relation, showing that the set adequately represents the expected size distribution of plankton in the natural environment (Sheldon et al., 1972).

https://doi.org/10.5194/essd-2026-614
Preprint. Discussion started: 2 September 2026

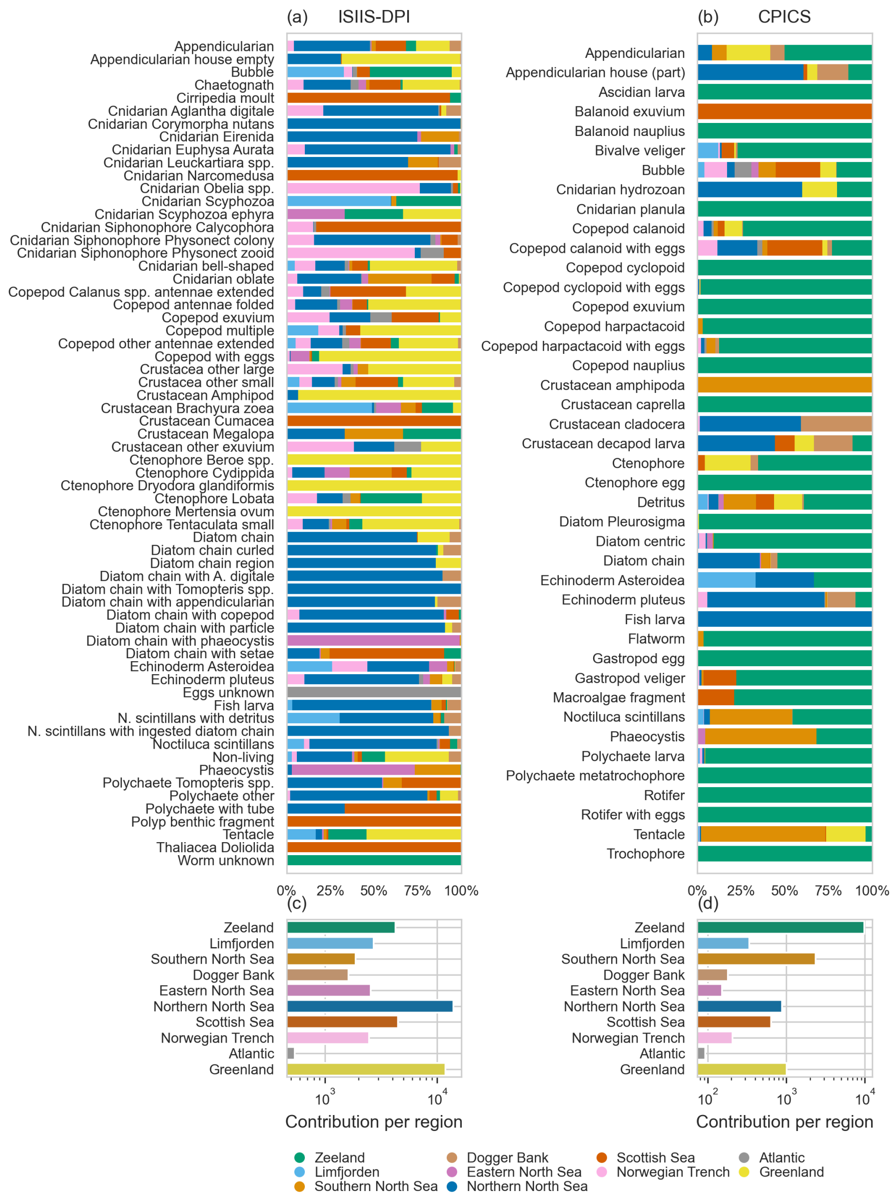

Figure 5. The origin of the annotated images of the ISIIS-DPI (a) and CPICS (b) according to the pelagic OSPAR Common Procedure Assessment Units for the Greater North Sea (Enserink et al., 2019). Panel c and d show the total number of annotated images per region for the ISIIS-DPI and CPICS, respectively. The colour-coding of the regions corresponds to Figure 1.

https://doi.org/10.5194/essd-2026-614
Preprint. Discussion started: 2 September 2026

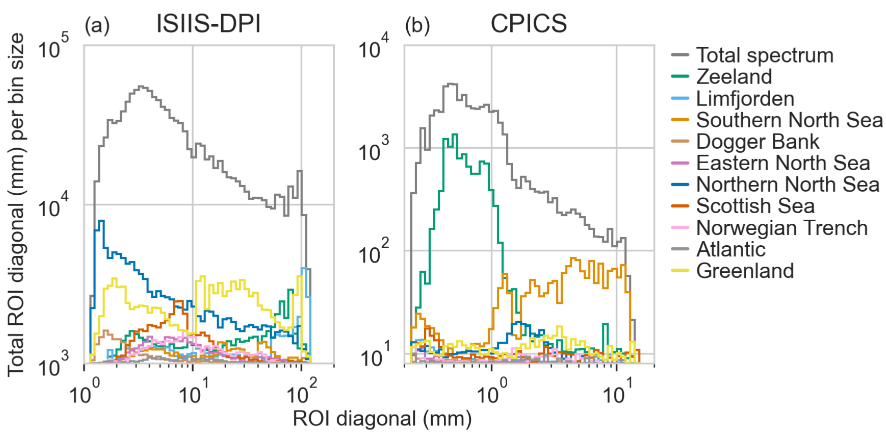

Figure 6. Normalized size spectrum of the annotated data of ISIIS-DPI (a) and CPICS (b) in which 'size' denotes the bounding box diagonal of an image (in mm). The coloured lines mark the relative contribution of a sampling region per size bin. Note the difference in scaling in the y direction: the total spectrum is plotted on a logarithmic scale, but the regional contributions per size bin are plotted on a linear scale, where in each size bin, a 100% contribution is marked by the y-position of the total (observed) spectrum. This means that if a region would contribute 50% of the observed images in a size bin, its curve would be halfway between the x-axis and the total observed spectrum for that size bin. The colour-coding of the regions corresponds to Figure 1.

3.1.3 Hydrographic conditions

The environmental conditions from which the images were collected are shown in Figure 7. Based on the median values of temperature, salinity, chlorophyll-a and depth, an evident end-member of the sampling conditions is the inshore area of Limfjorden and Zeeland, with high temperature (15 to 20 °C), low salinity (20 to 30 PSU), high chlorophyll-a concentrations (5 $\mu g\,L^{-1}$) and shallow depths (0 to 10 m). The Greenlandic fjords, Norwegian Trench and Atlantic show low temperature ($\sim$ 0 to 10 °) and low chlorophyll-a ($< 1\ \mu g\,L^{-1}$), and higher salinity (median $>$ 32 PSU). For these regions, salinity covers a wide range due to meltwater influence in Greenland (Hovenkamp et al., unpublished), and possibly due to run-off and Baltic influence in the sampling sites at the Norwegian Trench and the Atlantic (Otto et al., 1990). Greenland, the Norwegian Trench and Atlantic are also the only regions with images from below 100 m depth. The Southern, Eastern and Northern North Sea, Dogger Bank and Scottish Sea show a wide range of temperature and chlorophyll-a concentration in between the inshore and northern regions, but a narrow range of salinity ($>$ 34 PSU). Overall, the Greater North Sea covers near-shore areas, a large continental shelf and oceanic conditions, thus a broad range of hydrographic conditions can be expected. Figure 7 shows that these are well-represented within the annotated sets.

3.2 Classifier performance

For the ISIIS-DPI, the CNN classifier was trained on 52 classes (Figure 4a) and achieved an average precision, recall and F1-score of, respectively, 90.8%, 75.8% and 80.1% on the test set after probability filtering (Figure 8). For all classes except

https://doi.org/10.5194/essd-2026-614
Preprint. Discussion started: 2 September 2026

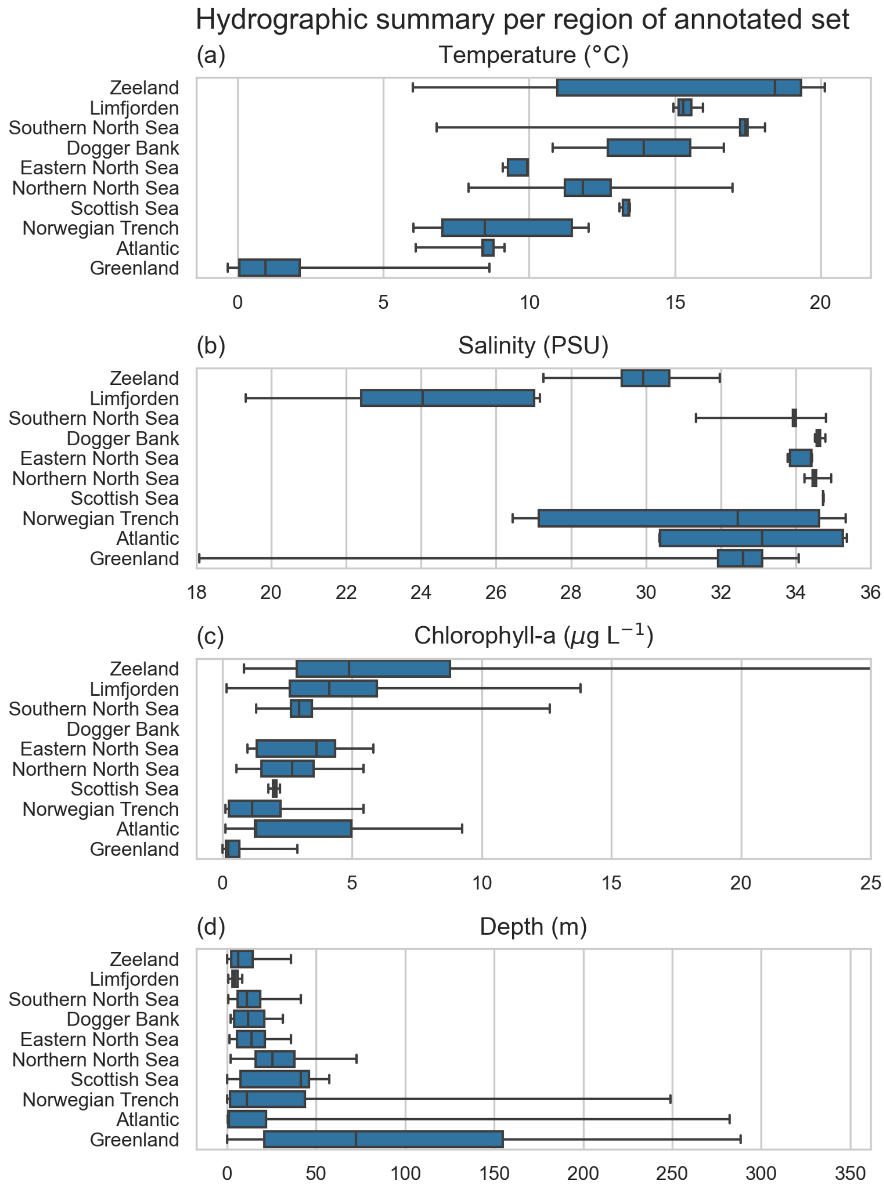

Figure 7. The temperature (a), salinity (b), chlorophyll-a concentration (c) and depth (d) from which the annotated images of the ISIIS-DPI and CPICS were collected per region.

https://doi.org/10.5194/essd-2026-614
Preprint. Discussion started: 2 September 2026

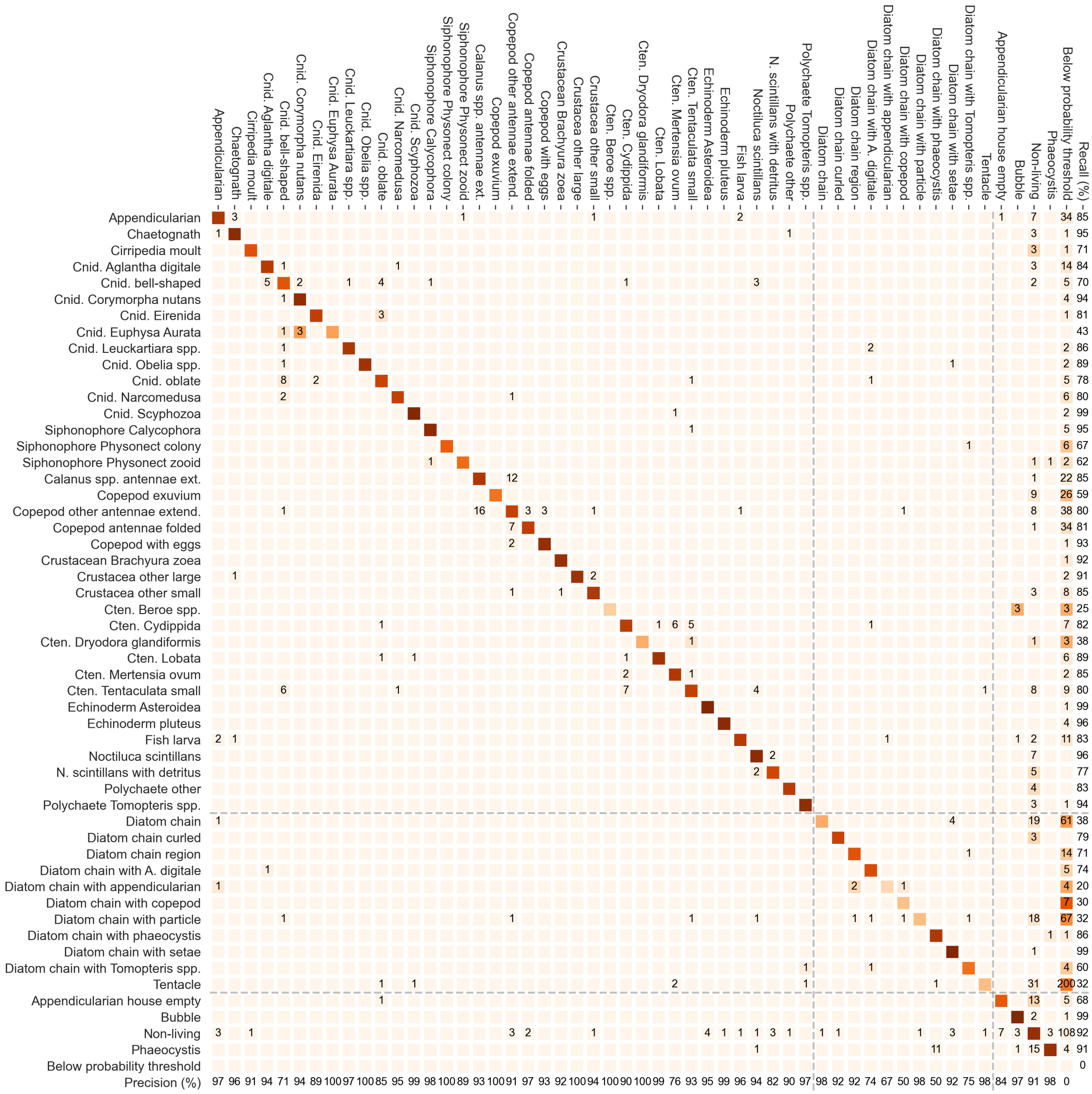

Figure 8. The confusion matrix of the ISIIS-DPI classifier evaluated on the ISIIS-DPI test set. Class names denote the predicted (x-axis) and ground truth labels (y-axis). The numbers indicate counts for each combination of predicted and ground truth class, except for the row and column named 'Precision' and 'Recall', respectively. Here, numbers denote the performance metric per class as percentage. Numbers on the diagonal are left out for enhanced visualization. The colour map denotes the counts of prediction-ground truth combinations relative to the number of ground truth images for a class. The dashed line indicates the grouping of classes used in the hierarchical loss function during training.

https://doi.org/10.5194/essd-2026-614
Preprint. Discussion started: 2 September 2026

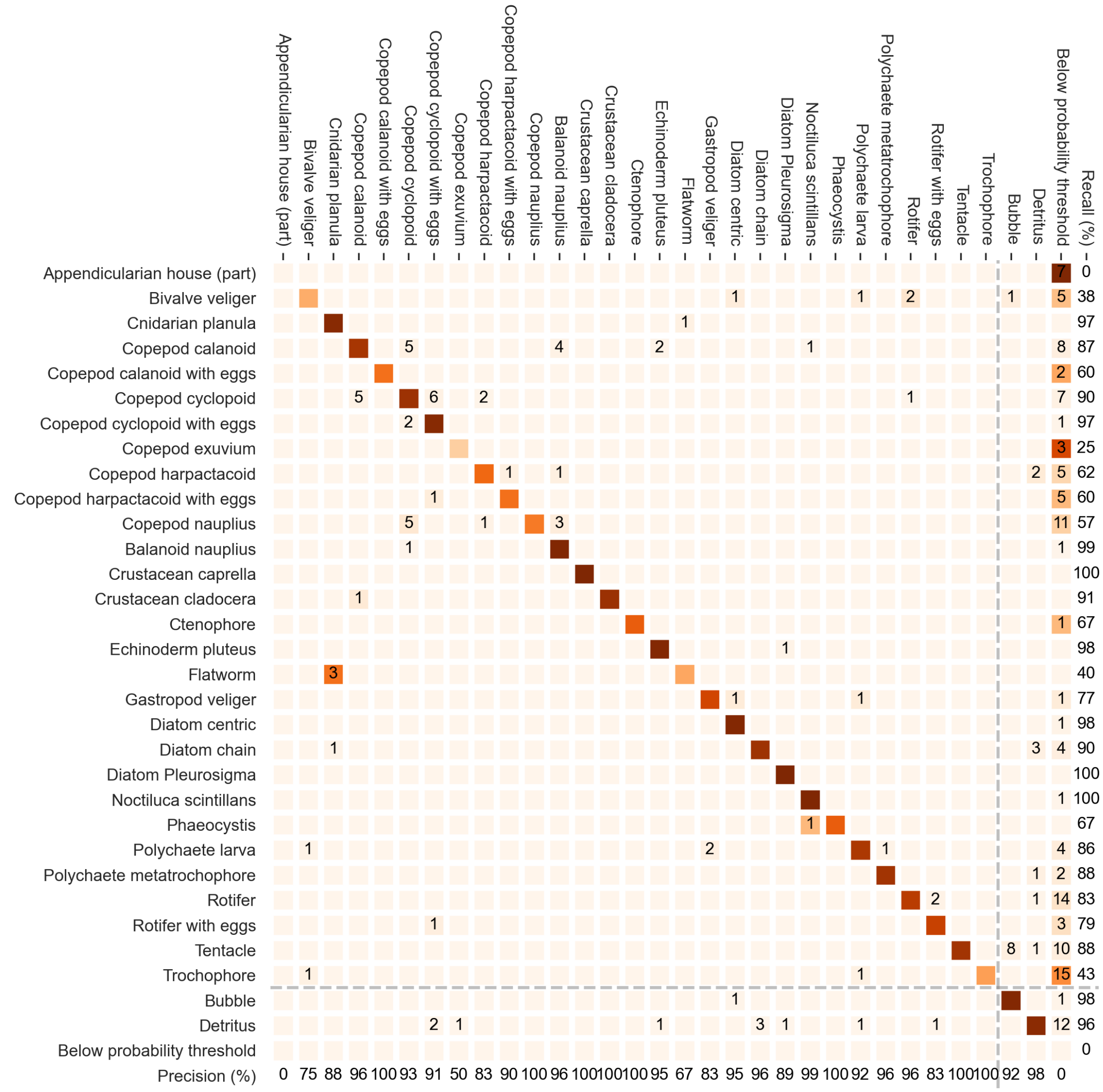

Figure 9. The confusion matrix of the CPICS classifier evaluated on the CPICS test set. The rest of the description is similar to Figure 8.

https://doi.org/10.5194/essd-2026-614
Preprint. Discussion started: 2 September 2026

the bell-shaped cnidarians, *Mertensia Ovum* and the classes with diatom chains, the precision was at least 80%, and for 39 classes the precision was above 90%. The probability filtering that we applied is a trade-off between increasing precision and decreasing precision (Faillettaz et al., 2016), and as a result, recall was substantially lower (20 to 99%) than precision. However, this can be corrected for by dividing the resulting taxon densities by the class-specific recall (Hu and Davis, 2006). Finally, it should be noted that the ISIIS-DPI data set consists of images of varying pixel resolution (17 and 38 µm). The fact that the classifier performance on the ISIIS-DPI set is comparable to the classifier from (e.g.) Hovenkamp et al. (2026a), which was trained on a data set with uniform pixel resolution (17 µm), suggests that the mix of pixel resolution within our set does not downgrade the classification performance. This means that within our annotated ISIIS-DPI set, no distinction by pixel resolution needs to be made when training or applying classifiers.

The CNN classifier of the CPICS data was trained on 31 classes (15,577 images). The average precision, recall and F1-score on the test set after probability filtering were 88.5%, 76.1% and 80.1% (Figure 9). The precision was at least 80% except for the classes ‘Copepod exuvium’, ‘Flatworm’, ‘Bivalve veliger’, and ‘Appendicularian house (part)’, of which the latter class is missed completely after probabity filtering. The recall of the CPICS classifier varied between 25% and 100% (except for ‘Appendicularian house part’), but for 22 classes, the precision was higher than 90%. The observed classifier errors (Figure 9) within the CPICS copepod classes may be a result of the on-board segmentation, which, as we observed, commonly cuts off the antennae of copepods.

4 Outlook

Public sharing of expert-annotated image datasets was identified as a bottleneck for the application of image processing pipelines by various authors (Irisson et al., 2022; Orenstein et al., 2022). Here, we presented a large, annotated set of images from the ISIIS-DPI (46,331) and CPICS (14,496), and showed that this set is representative for the Greater North Sea region based on geographical coverage, environmental data and size distribution. In addition, we trained two CNNs with precision of 90.8% (ISIIS-DPI) and 88.5% (CPICS) that can be used for reliable classification of newly collected data within the Greater North Sea. By taking subsets or aggregations of the annotated sets, users can create their own learning set and train a new classifier that best fits their use-case.

Future work may further expand the size and taxonomic detail of the set that we presented. For example, the geographical coverage of the set could be further improved by including more sites in the Northern and Eastern North Sea, from which only the boundary regions were sampled (Figure 1). However, since these areas are predominantly influenced by water masses passing from the Atlantic along the North-East of Scotland or along the western edge of the Norwegian Trench (Krause et al., 1995), we argue that zooplankton of the Northern and Eastern North Sea is nevertheless reasonably covered. We hope that this work will prove valuable for research groups working in the field of in situ imaging in the Greater North Sea.

https://doi.org/10.5194/essd-2026-614
Preprint. Discussion started: 2 September 2026

Open Access Earth System Science Data Discussions

Code and data availability. The presented data, CNN classifiers and Python code used for CNN training and usage are available at 10.5281/zenodo.21737141 (Hovenkamp et al., 2026c).

265 *Author contributions.* PH, AFvdS and DvO conceived and designed the study with input from DT and LvW. PH, DvO, DT and LvW collected the field data. PH and LvW manually labelled the images. PH performed the data analysis and programming. PH wrote the manuscript with the support of AFvdS and DvO and with significant input from all authors. AFvdS and DvO supervised the study.

Competing interests. The authors declare that they have no conflict of interest.

Acknowledgements. This study was made possible through collaborative funding between Utrecht University, the Netherlands, and the
270 Royal Netherlands Institute for Sea Research (NIOZ). We would like to thank the crew of all research vessels – RV Navicula, RV Pelagia, RV Belgica and RV Egon P – that enabled one or more of the sampling campaigns from this study, and Anton Tramper and Jeroen van Dalen for sailing the RV Zeevonk in the Zeeland campaigns and for assistance on many research cruises. Cornelia Jaspers kindly invited us on a sampling campaign in Limfjorden, and Hannah Kepner helped with identifications of jellyfish. Furu Mienis provided valuable input on this manuscript. Loek Bijl and Elena Tasoula assisted in data collection during one of the North Sea cruises in 2022.

https://doi.org/10.5194/essd-2026-614
Preprint. Discussion started: 2 September 2026

Appendix A

https://doi.org/10.5194/essd-2026-614
Preprint. Discussion started: 2 September 2026

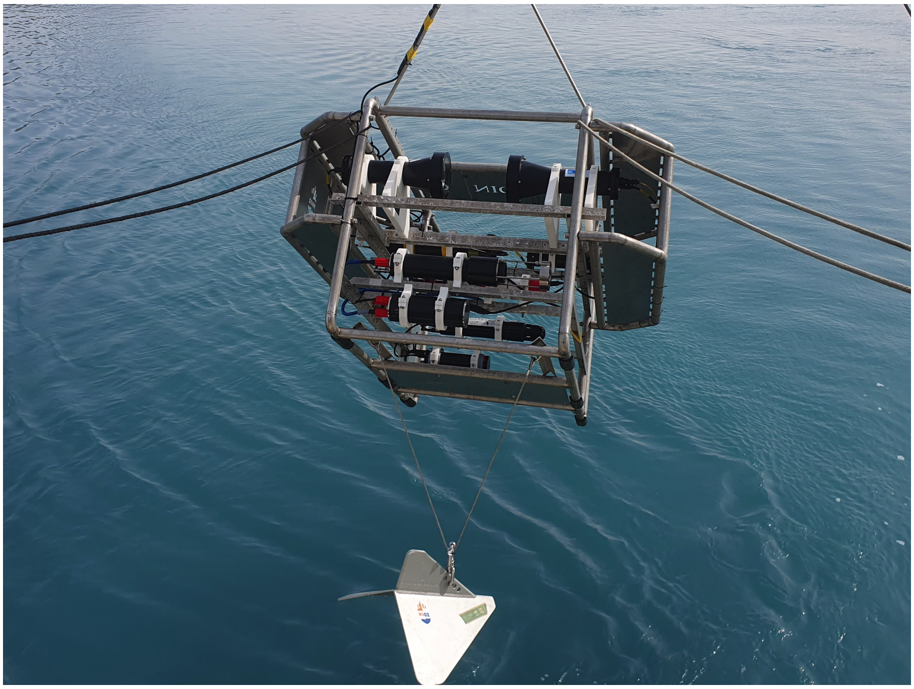

Figure A1. The modular Deep-focus Plankton Imager (ISIIS-DPI), Continuous Plankton Imaging and Classification Sensor (CPICS) and various other sensors mounted on the towed frame before a deployment.

https://doi.org/10.5194/essd-2026-614
Preprint. Discussion started: 2 September 2026

References

Ahyong, S., Boyko, C., Bernot, J., Brandão, S., Daly, M., De Grave, S., de Voogd, N., Gofas, S., Hernandez, F., Mees, J., Neubauer, T., Paulay, G., van der Meij, S., Boydens, B., Dekeyzer, S., Goharimanesh, M., Vandepitte, L., Vanhoorne, B., Ackerfield, J., Agatha, S., Ahn, K., Alvarez, B., Alves, K., Amler, M., Amorim, V., Anderberg, A., Andrés-Sánchez, S., Andriamanohera, M., Ang, Y., Antić, D., Antonietto, L., Anzuinelli, M., Arango, C., Ariño, A., Artois, T., Atkinson, S., Auffenberg, K., Avila, F., Bailly, N., Baldwin, B., Bank, R., Baquero, E., Barber, A., Barbosa, M., Barrett, R., Bartsch, I., Bergh, N., Bernard, C., Berrios Ortega, F., Berta, A., Bezerra, T., Bhandari, P., Bieler, R., Blanco, S., Blanco Gavaldà, C., Blasco-Costa, I., Blazewicz, M., Bledzki, L., Bock, P., Bonifacino, M., Böttger-Schnack, R., Bouchet, P., Boury-Esnault, N., Bouzan, R., Boxshall, G., Bradshaw, C., Bray, R., Browning, J., Bruce, N., Bruhl, J., Bruneau, A., Budaeva, N., Bueno-Villegas, J., Buhaug, M., Burkhardt, U., Calvo Casas, J., Campos-Filho, I., Cárdenas, P., Carstens, E., Carvalho, A., Cavalcante Bellini, B., Cedhagen, T., Chan, B., Chan, T., Cheng, H., Chernyshev, A., Choong, H., Christenhusz, M., Churchill, M., Collins, A., Collins, G., Collins, K., Consorti, L., Copilaș-Ciocianu, D., Corbari, L., Cordeiro, R., Costa, S., Costa Corgosinho, P., Coste, M., Cramphorn, B., Crandall, K., Cremonte, F., Cribb, T., Cutmore, S., Dahdouh-Guebas, F., Daneliya, M., Dauvin, J., Davie, P., De Broyer, C., de Lima Ferreira, P., de Mazancourt, V., de Moura Oliveira, L., Decker, P., Defaye, D., Dekker, H., DeSalle, R., Di Capua, I., Diazgranados, M., Dippenaar, S., Dohrmann, M., Dolan, J., Domning, D., D'Onofrio, R., Downey, R., Dreyer, N., Duke, N., Eisendle, U., Eleaume, M., Elliott, T., Enghoff, H., Epler, J., Esquete Garrote, P., Evenhuis, N., Ewers-Saucedo, C., Faber, M., Farias, A., Figueroa, D., Figuerola, B., Fišer, C., Ford, B., Ford, K., Fordyce, E., Foster, W., Fransen, C., Freire, S., Fujimoto, S., Furuya, H., Galbany-Casals, M., Gale, A., Gao, T., García Rodríguez, R., García-Moro, P., Garic, R., Garnett, S., Gaviria-Melo, S., Gebauer, S., Gellert, M., Gerken, S., Gibson, D., Gil, A., Gil, J., Gittenberger, A., Glasby, C., Glenner, H., Glover, A., Goetghebeur, P., Gómez-Noguera, S., Gondim, A., Gonzalez, B., González-Elizondo, M., González-Gallego, L., González-Solís, D., Goodwin, C., Gostel, M., Grabowski, M., Grossi, M., Guerra-García, J., Guerrero, J., Guidetti, R., Guiry, M., Gutierrez, D., Hadfield, K., Hajdu, E., Halanych, K., Hallermann, J., Hasenhütl, K., Hayward, B., Hegna, T., Heiden, G., Hendrycks, E., Hennen, D., Henriques Santana, M., Herbert, D., Hipp, A., Hodda, M., Høeg, J., Hoeksema, B., Holovachov, O., Hooge, M., Hooper, J., Horton, T., Hoshino, T., Houart, R., Hroudová, Z., Hughes, L., Hughes, T., Huys, R., Hyžný, M., Iniesta, L., Iseto, T., Iwataki, M., Janssen, R., Jaume, D., Jazdzewski, K., Jersabek, C., Jiménez-Mejías, P., Jin, X., Johnson da Silva, W., Johnsson, R., Jordana, R., Jóźwiak, P., Jung, M., Kabat, A., Kajihara, H., Kakui, K., Kantor, Y., Karapunar, B., Karthick, B., Kasai, H., Kathirithamby, J., Katinas, L., Katz, A., Kilian, N., Kim, S., Kim, Y., King, R., Kirk, P., Klautau, M., Kmentova, N., Kociolek, J., Koekemoer, M., Köhler, F., Konowalik, K., Kotov, A., Kovac, L., Kovács, Z., Kremenetskaia, A., Kristensen, R., Kroh, A., Kulikovskiy, M., Kullander, S., Kupriyanova, E., Lacroix-Carignan, , Lamaro, A., Lambert, G., Larridon, I., Lazarus, D., Le Coze, F., Le Roux, M., Leal, M., LeCroy, S., Leduc, D., Lefkowitz, E., Lemaitre, R., Léveillé-Bourret, , Licher, M., Lichter-Marck, I., Lim, S., Lindsay, D., Liu, Y., Loeuille, B., Lois, R., Lörz, A., Lu, Y., Luceño Garcés, M., Ludwig, T., Lundholm, N., Maciel Silva, J., Macpherson, E., Mah, C., Mamos, T., Manconi, R., Mandel, J., Mańko, M., Mapstone, G., Marco Rosado, N., Marek, P., Marhold, K., Markello, K., Marques, L., Márquez-Corro, J., Marshall, B., Marshall, D., Martin, P., Martín-Bravo, S., Martinez Arbizu, P., Masaki, T., Maslakova, S., Mateos, E., Mauricio, R., McFadden, C., McInnes, S., McKenzie, R., Means, J., Mejía-Madrid, H., Meland, K., Merrin, K., Mesterházy, A., Míguez, M., Miller, J., Mills, C., Miranda, L., Mokievsky, V., Molodtsova, T., Mooi, R., Moore-Pollard, E., Morales, D., Morales-Alonso, A., Morandini, A., Moreira da Rocha, R., Morel, J., Moreyra C., L., Moritz, L., Morrow, C., Mortelmans, J., Muasya, M., Müller, A., Muñoz Gallego, A., Muñoz Schüler, P., Musco, L., Naczi, R., Nesom, G., Neubert, E., Neuhaus, B., Ng, P., Nguyen, A., Nielsen, S., Nishikawa, T., Norenburg, J., Nunes, C., Nunes Godeiro, N., Oberprieler, C., O'Hara, T., Opresko, D., Osawa, M., Osigus, H., Ota, Y., Oyebanji, O., Páll-Gergely, B., Panero, J., Parra-Gómez, A., Passarelli, J., Patterson, D., Peart, R., Pedram, M., Pelser, P., Peña Santiago, R., Perbiche-Neves, G., Pereira, J., Pereira, S., Pereira-Silva, L., Perez-Losada, M., Petrescu, I., Pfingstl, T., Phelan, N., Piasecki, W., Pica, D., Picton, B., Pignatti, J., Pilger, J., Pinheiro, U., Pisera, A., Poatskievick Pierezan, B., Pohle, A., Poindexter, D., Polhemus, D., Poore, G., Potapov, A., Potapova, M., Praxedes, R., Půža, V., Ramírez, A., Rasaminirina, F., Read, G., Reich, M., Reid, J., Reimer, J., Reip, H., Remor, D., Resende Bueno, V., Reuscher, M., Reynolds, J., Reznicek, A., Richling, I., Rimet, F., Rink, G., Ríos, P., Rius, M., Rodríguez, E., Rogers, D., Rosenberg, G., Ross, G., Sá, H., Saavedra, M., Sabater, L., Sabbe, K., Sabroux, R., Saiz-Salinas, J., Sala, S., Samimi-Namin, K., Sánchez Santos, N., Sánchez-Villegas, R., Santagata, S., Santos, S., Santos Filho, M., Sanz Arnal, M., Sar, E., Saucède, T., Schärer, L., Schierwater, B., Schilling, E., Schmidt-Lebuhn, A., Schneider, C., Schneider, L., Schneider, S., Schönberg, C., Schrével, J., Schweitzer, C., Segers, H., Semple, J., Senna, A., Sennikov, A., Serejo, C., Shaik, S., Shamsi, S., Sharma, J., Sharma, J., Shear, W., Shenkar, N., Short, M., Sicinski, J., Sierwald, P., Silva da Silva Filho, P., Simmons, E., Simpson, D., Siniscalchi, C., Sinniger, F., Sinou, C., Sivell, D., Smit, H., Smit, N., Smol, N., Sørensen, M., Souza-Filho, J., Spalink, D., Spelda, J., Starr, J., Sterrer, W., Steyn, H., Stoev, P., Stöhr, S., Suárez-Morales, E., Susanna, A., Suttle, C., Swalla, B., Szubryt, M., Takahashi, K., Tanaka, M., Tandberg, A., Tang, D., Tasker, M., Taylor, J., Taylor, J., Taylor, K., Tchesunov, A., Temereva, E., ten Hove, H., ter Poorten, J., Thirouin, K., Thomas, J., Thomas, W., Thuesen, E., Thurston, M., Thuy, B., Timi, J., Todaro, A., Todd, J., Tomasello, S., Trevisan Disaró, S., Tucker, G., Turon, X., Tyler, S., Uetz, P., Urbatsch, L., Uribe-Palomino, J., Urtubey, E., Utevsky, S., Uy, M., Vacelet, J., Vader, W., Väinölä, R., Valdés Florido, A., Valls Domedel, G., Van de Vijver, B., van Haaren, T., van Soest, R., Vázquez-García, B., Venekey, V., Verhoeff, T., Verloove, F., Vinarski, M., Volkova, P., Vonk, R., Vos, C., Vouilloud, A., Walker-Smith, G., Walter, T., Watling, L., Wayland, M., Wesener, T., Wetzel, C., Whipps, C., White, K., Wieneke, U., Williams, D., Williams, G., Williams, N., Wilson, K., Wilson, R., Witkowski, J., Wood, T., Woudstra, Y., Xanthos, M., Xavier, J., Xu, K., Yano, O., Yu, D., Zanol, J., Zeidler, W., Zhang, S., Zhao, Z., and Zullini, A.: World Register of Marine Species (WoRMS), https://doi.org/10.14284/170, 2026.

Atkinson, A., Lilley, M. K., Hirst, A. G., McEvoy, A. J., Tarran, G. A., Widdicombe, C., Fileman, E. S., Woodward, E. M. S., Schmidt, K., Smyth, T. J., and Somerfield, P. J.: Increasing nutrient stress reduces the efficiency of energy transfer through planktonic size spectra, Limnology and Oceanography, 66, 422–437, https://doi.org/10.1002/lno.11613, 2021.

Atkinson, A., Rossberg, A. G., Gaedke, U., Sprules, G., Heneghan, R. F., Batziakas, S., Grigoratou, M., Fileman, E., Schmidt, K., and Frangoulis, C.: Steeper size spectra with decreasing phytoplankton biomass indicate strong trophic amplification and future fish declines, Nature Communications, 15, 381, https://doi.org/10.1038/s41467-023-44406-5, 2024.

Batten, S., Clark, R., Flinkman, J., Hays, G., John, E., John, A., Jonas, T., Lindley, J., Stevens, D., and Walne, A.: CPR sampling: the technical background, materials and methods, consistency and comparability, Progress in Oceanography, 58, 193–215, https://doi.org/10.1016/j.pocean.2003.08.004, 2003.

Bertinetto, L., Mueller, R., Tertikas, K., Samangooei, S., and Lord, N. A.: Making Better Mistakes: Leveraging Class Hierarchies With Deep Networks, in: 2020 IEEE/CVF Conference on Computer Vision and Pattern Recognition (CVPR), pp. 12 503–12 512, IEEE, Seattle, WA, USA, ISBN 978-1-7281-7168-5, https://doi.org/10.1109/CVPR42600.2020.01252, 2020.

Bochinski, E., Bacha, G., Eiselein, V., Walles, T. J. W., Nejstgaard, J. C., and Sikora, T.: Deep Active Learning for In Situ Plankton Classification, in: Pattern Recognition and Information Forensics, edited by Zhang, Z., Suter, D., Tian, Y., Branzan Albu, A., Sidère, N., and Jair Escalante, H., pp. 5–15, Springer International Publishing, Cham, ISBN 978-3-030-05792-3, 2019.

Canny, J.: A Computational Approach to Edge Detection, IEEE Transactions on Pattern Analysis and Machine Intelligence, PAMI-8, 679–698, https://doi.org/10.1109/TPAMI.1986.4767851, 1986.

Capuzzo, E., Lynam, C. P., Barry, J., Stephens, D., Forster, R. M., Greenwood, N., McQuatters-Gollop, A., Silva, T., van Leeuwen, S. M., and Engelhard, G. H.: A decline in primary production in the North Sea over 25 years, associated with reductions in zooplankton abundance and fish stock recruitment, Global Change Biology, 24, e352–e364, https://doi.org/10.1111/gcb.13916, 2018.

Cowen, R. K. and Guigand, C. M.: In situ ichthyoplankton imaging system (ISIIS): system design and preliminary results: In situ ichthyoplankton imaging system, Limnology and Oceanography: Methods, 6, 126–132, https://doi.org/10.4319/lom.2008.6.126, 2008.

Deng, J., Dong, W., Socher, R., Li, L.-J., Li, K., and Fei-Fei, L.: ImageNet: A large-scale hierarchical image database, in: 2009 IEEE Conference on Computer Vision and Pattern Recognition, pp. 248–255, https://doi.org/10.1109/CVPR.2009.5206848, 2009.

Desmit, X., Nohe, A., Borges, A. V., Prins, T., De Cauwer, K., Lagring, R., Van Der Zande, D., and Sabbe, K.: Changes in chlorophyll concentration and phenology in the North Sea in relation to de-eutrophication and sea surface warming, Limnology and Oceanography, 65, 828–847, https://doi.org/10.1002/lno.11351, 2020.

Drinkwater, K. F., Belgrano, A., Borja, A., Conversi, A., Edwards, M., Greene, C. H., Ottersen, G., Pershing, A. J., and Walker, H.: The Response of Marine Ecosystems to Climate Variability Associated with the North Atlantic Oscillation, in: The North Atlantic Oscillation: Climatic Significance and Environmental Impact, Geophysical Monograph Series, pp. 211–234, ISBN 978-1-118-66903-7, https://doi.org/10.1029/134GM10, 2003.

Dye, S., Hughes, S., Tinker, J., Berry, D., Holliday, N., Kent, E., Kennington, K., Inall, M., Smyth, T., Nolan, G., Lyons, K., Andres, O., and Beszczynska-Moeller, A.: Impacts of climate change on temperature (air and sea), MCCIP Science Review 2013, pp. 1–12, https://doi.org/10.14465/2013.arc01.001-012, 2013.

Eerola, T., Batrakhanov, D., Barazandeh, N. V., Kraft, K., Haraguchi, L., Lensu, L., Suikkanen, S., Seppälä, J., Tamminen, T., and Kälviäinen, H.: Survey of automatic plankton image recognition: challenges, existing solutions and future perspectives, Artificial Intelligence Review, 57, 114, https://doi.org/10.1007/s10462-024-10745-y, 2024.

Emeis, K.-C., Van Beusekom, J., Callies, U., Ebinghaus, R., Kannen, A., Kraus, G., Kröncke, I., Lenhart, H., Lorkowski, I., Matthias, V., Möllmann, C., Pätsch, J., Scharfe, M., Thomas, H., Weisse, R., and Zorita, E.: The North Sea — A shelf sea in the Anthropocene, Journal of Marine Systems, 141, 18–33, https://doi.org/10.1016/j.jmarsys.2014.03.012, 2015.

Enserink, L., Blauw, A., van der Zande, D., and Markager, S.: Summary report of the EU project 'Joint monitoring programme of the eutrophication of the North Sea with satellite data' (Ref: DG ENV/MSFD Second Cycle/2016), Tech. rep., 2019.

Faillettaz, R., Picheral, M., Luo, J. Y., Guigand, C., Cowen, R. K., and Irisson, J.-O.: Imperfect automatic image classification successfully describes plankton distribution patterns, Methods in Oceanography, 15-16, 60–77, https://doi.org/10.1016/j.mio.2016.04.003, 2016.

Floeter, J., Van Beusekom, J. E., Auch, D., Callies, U., Carpenter, J., Dudeck, T., Eberle, S., Eckhardt, A., Gloe, D., Hänselmann, K., Hufnagl, M., Janßen, S., Lenhart, H., Möller, K. O., North, R. P., Pohlmann, T., Riethmüller, R., Schulz, S., Spreizenbarth, S., Temming, A., Walter, B., Zielinski, O., and Möllmann, C.: Pelagic effects of offshore wind farm foundations in the stratified North Sea, Progress in Oceanography, 156, 154–173, https://doi.org/10.1016/j.pocean.2017.07.003, 2017.

Forest, A., Stemmann, L., Picheral, M., Burdorf, L., Robert, D., Fortier, L., and Babin, M.: Size distribution of particles and zooplankton across the shelf-basin system in southeast Beaufort Sea: combined results from an Underwater Vision Profiler and vertical net tows, Biogeosciences, 9, 1301–1320, https://doi.org/10.5194/bg-9-1301-2012, 2012.

Gallager, S. M.: The Continuous Plankton Imaging and Classification Sensor (CPICS): A Sensor for Quantifying Mesoplankton Biodiversity and Community Structure, in: American Geophysical Union, vol. 2016, pp. IS52A–07, 2016.

Greer, A. T., Cowen, R. K., Guigand, C. M., and Hare, J. A.: Fine-scale planktonic habitat partitioning at a shelf-slope front revealed by a high-resolution imaging system, Journal of Marine Systems, 142, 111–125, https://doi.org/10.1016/j.jmarsys.2014.10.008, 2015.

Greer, A. T., Duffy, P. I., Walles, T. J. W., Cousin, C., Treible, L. M., Aaron, K. D., and Nejstgaard, J. C.: Modular shadowgraph imaging for zooplankton ecological studies in diverse field and mesocosm settings, Limnology and Oceanography: Methods, 23, 67–86, https://doi.org/10.1002/lom3.10657, 2025.

Grosjean, P., Picheral, M., Warembourg, C., and Gorsky, G.: Enumeration, measurement, and identification of net zooplankton samples using the ZOOSCAN digital imaging system, Ices Journal of Marine Science, 61, 518–525, https://doi.org/10.1016/j.icesjms.2004.03.012, wOS:000222322500010, 2004.

Holland, M., Louchart, A., Artigas, L. F., and McQuatters-Gollop, A.: OSPAR's Quality Status Report 2023 PH1/FW5 Changes in phytoplankton and zooplankton communities, 2023.

Horton, T., Marsh, L., Bett, B. J., Gates, A. R., Jones, D. O. B., Benoist, N. M. A., Pfeifer, S., Simon-Lledó, E., Durden, J. M., Vandepitte, L., and Appeltans, W.: Recommendations for the Standardisation of Open Taxonomic Nomenclature for Image-Based Identifications, Frontiers in Marine Science, 8, 620 702, https://doi.org/10.3389/fmars.2021.620702, 2021.

Hovenkamp, P. D. L., Meire, L., Soetaert, K., van der Stappen, A. F., and Van Oevelen, D.: Resolving the fine-scale zooplankton distribution in relation to glacial discharge in two contrasting southern Greenlandic fjords with automated in situ imaging, Submitted to Marine Ecology Progress Series.

Hovenkamp, P. D. L., Peck, M. A., van der Stappen, A. F., and van Oevelen, D.: Strong spatial partitioning of mesozooplankton in a dynamic frontal zone shapes trophic transfer efficiency, Limnology and Oceanography, 71, e70 453, https://doi.org/10.1002/lno.70453, 2026a.

Hovenkamp, P. D. L., van Walraven, L., Ollevier, A., van Oevelen, D., and van der Stappen, A. F.: Optimizing automated classification for zooplankton in coastal conditions: the impact of model selection, imaging instruments, and colour information, bioRxiv, p. 2026.07.09.733739, https://doi.org/10.64898/2026.07.09.733739, 2026b.

Hovenkamp, P. D. L., Van Walraven, L., Temmerman, D., van der Stappen, A. F., and Van Oevelen, D.: A FAIR annotated set of 60k+ in situ zooplankton images from the Greater North Sea and Greenland [Data set], https://doi.org/10.5281/zenodo.21737141, 2026c.

Hu, Q. and Davis, C.: Accurate automatic quantification of taxa-specific plankton abundance using dual classification with correction, Marine Ecology Progress Series, 306, 51–61, https://doi.org/10.3354/meps306051, 2006.

Irisson, J.-O., Ayata, S.-D., Lindsay, D. J., Karp-Boss, L., and Stemmann, L.: Machine Learning for the Study of Plankton and Marine Snow from Images, Annual Review of Marine Science, 14, 277–301, https://doi.org/10.1146/annurev-marine-041921-013023, 2022.

Isaksson, N., Scott, B. E., Hunt, G. L., Benninghaus, E., Declerck, M., Gormley, K., Harris, C., Sjöstrand, S., Trifonova, N. I., Waggitt, J. J., Wihsgott, J. U., Williams, C., Zampollo, A., and Williamson, B. J.: A paradigm for understanding whole ecosystem effects of offshore wind farms in shelf seas, ICES Journal of Marine Science, 82, fsad194, https://doi.org/10.1093/icesjms/fsad194, 2025.

Krause, M., Dippner, J. W., and Beil, J.: A review of hydrographic controls on the distribution of zooplankton biomass and species in the North Sea with particular reference to a survey conducted in January–March 1987, Progress in Oceanography, 35, 81–152, https://doi.org/10.1016/0079-6611(95)00006-3, 1995.

Luo, J., Grassian, B., Tang, D., Irisson, J., Greer, A., Guigand, C., McClatchie, S., and Cowen, R.: Environmental drivers of the fine-scale distribution of a gelatinous zooplankton community across a mesoscale front, Marine Ecology Progress Series, 510, 129–149, https://doi.org/10.3354/meps10908, 2014.

Luo, J. Y., Irisson, J., Graham, B., Guigand, C., Sarafraz, A., Mader, C., and Cowen, R. K.: Automated plankton image analysis using convolutional neural networks, Limnology and Oceanography: Methods, 16, 814–827, https://doi.org/10.1002/lom3.10285, 2018.

McQuatters-Gollop, A., Guérin, L., Arroyo, N., Aubert, A., Artigas, L., Bedford, J., Corcoran, E., Dierschke, V., Elliott, S., Geelhoed, S., Gilles, A., González-Irusta, J., Haelters, J., Johansen, M., Le Loc'h, F., Lynam, C., Niquil, N., Meakins, B., Mitchell, I., Padegimas, B., Pesch, R., Preciado, I., Rombouts, I., Safi, G., Schmitt, P., Schückel, U., Serrano, A., Stebbing, P., De La Torriente, A., and Vina-Herbon, C.: Assessing the state of marine biodiversity in the Northeast Atlantic, Ecological Indicators, 141, 109 148, https://doi.org/10.1016/j.ecolind.2022.109148, 2022.

Orenstein, E. C., Ayata, S., Maps, F., Becker, C., Benedetti, F., Biard, T., de Garidel-Thoron, T., Ellen, J. S., Ferrario, F., Giering, S. L. C., Guy-Haim, T., Hoebeke, L., Iversen, M. H., Kiørboe, T., Lalonde, J., Lana, A., Laviale, M., Lombard, F., Lorimer, T., Martini, S., Meyer, A., Möller, K. O., Niehoff, B., Ohman, M. D., Pradalier, C., Romagnan, J., Schröder, S., Sonnet, V., Sosik, H. M., Stemmann, L. S., Stock, M., Terbiyik-Kurt, T., Valcárcel-Pérez, N., Vilgrain, L., Wacquet, G., Waite, A. M., and Irisson, J.: Machine learning techniques to characterize functional traits of plankton from image data, Limnology and Oceanography, 67, 1647–1669, https://doi.org/10.1002/lno.12101, 2022.

Otto, L., Zimmerman, J., Furnes, G., Mork, M., Saetre, R., and Becker, G.: Review of the physical oceanography of the North Sea, Netherlands Journal of Sea Research, 26, 161–238, https://doi.org/10.1016/0077-7579(90)90091-T, 1990.

Quante, M. and Colijn, F., eds.: North Sea Region Climate Change Assessment, Regional Climate Studies, Springer International Publishing, Cham, ISBN 978-3-319-39743-6 978-3-319-39745-0, https://doi.org/10.1007/978-3-319-39745-0, 2016.

Remsen, A., Hopkins, T. L., and Samson, S.: What you see is not what you catch: a comparison of concurrently collected net, Optical Plankton Counter, and Shadowed Image Particle Profiling Evaluation Recorder data from the northeast Gulf of Mexico, Deep Sea Research Part I: Oceanographic Research Papers, 51, 129–151, https://doi.org/10.1016/j.dsr.2003.09.008, 2004.

Richardson, A. J.: In hot water: zooplankton and climate change, ICES Journal of Marine Science, 65, 279–295, https://doi.org/10.1093/icesjms/fsn028, 2008.

Rohr, T., Richardson, A. J., Lenton, A., Chamberlain, M. A., and Shadwick, E. H.: Zooplankton grazing is the largest source of uncertainty for marine carbon cycling in CMIP6 models, Communications Earth & Environment, 4, 212, https://doi.org/10.1038/s43247-023-00871-w, 2023.

Schmid, M. S., Cowen, R. K., Robinson, K., Luo, J. Y., Briseño-Avena, C., and Sponaugle, S.: Prey and predator overlap at the edge of a mesoscale eddy: fine-scale, in-situ distributions to inform our understanding of oceanographic processes, Scientific Reports, 10, 921, https://doi.org/10.1038/s41598-020-57879-x, 2020.

Schmid, M. S., Sponaugle, S., Thompson, A. W., Sutherland, K. R., and Cowen, R. K.: Drivers of plankton community structure in intermittent and continuous coastal upwelling systems–from microbes and microscale in-situ imaging to large scale patterns, Frontiers in Marine Science, 10, 1166 629, https://doi.org/10.3389/fmars.2023.1166629, 2023.

Schröder, S.-M., Kiko, R., Irisson, J.-O., and Koch, R.: Low-Shot Learning of Plankton Categories, in: Pattern Recognition, edited by Brox, T., Bruhn, A., and Fritz, M., pp. 391–404, Springer International Publishing, Cham, ISBN 978-3-030-12939-2, 2019.

Sheldon, R. W., Prakash, A., and Sutcliffe, W. H.: The Size Distribution of Particles in the Ocean, Limnology and Oceanography, 17, 327–340, https://doi.org/10.4319/lo.1972.17.3.0327, 1972.

Simpson, S., Jennings, S., Johnson, M., Blanchard, J., Schön, P.-J., Sims, D., and Genner, M.: Continental Shelf-Wide Response of a Fish Assemblage to Rapid Warming of the Sea, Current Biology, 21, 1565–1570, https://doi.org/10.1016/j.cub.2011.08.016, 2011.

Steinberg, D. K. and Landry, M. R.: Zooplankton and the Ocean Carbon Cycle, Annual Review of Marine Science, 9, 413–444, https://doi.org/10.1146/annurev-marine-010814-015924, 2017.

Tan, M. and Le, Q.: EfficientNetV2: Smaller Models and Faster Training, in: Proceedings of the 38th International Conference on Machine Learning, edited by Meila, M. and Zhang, T., vol. 139 of *Proceedings of Machine Learning Research*, pp. 10 096–10 106, PMLR, https://proceedings.mlr.press/v139/tan21a.html, 2021.

https://doi.org/10.5194/essd-2026-614
Preprint. Discussion started: 2 September 2026

Taylor, A. H., Allen, J. I., and Clark, P. A.: Extraction of a weak climatic signal by an ecosystem, Nature, 416, 629–632, https://doi.org/10.1038/416629a, 2002.

Van Leeuwen, S., Tett, P., Mills, D., and Van Der Molen, J.: Stratified and nonstratified areas in the North Sea: Long-term variability and biological and policy implications, Journal of Geophysical Research: Oceans, 120, 4670–4686, https://doi.org/10.1002/2014JC010485, 2015.

Van Walraven, L., Scott, J., Pitois, S., Ribeiro, J., Close, H., Pettigrew, J., Liszka, C. M., Fileman, E., Hoekendijk, J., Hovenkamp, P., Jak, R., Van Dalen, J., and Van Oevelen, D.: PlanktoShare: A large (50k+) and FAIR learning set for the Plankton Imager (Pi-10) for the Greater North Sea and NE Atlantic, based on a new flexible classification protocol, https://doi.org/10.5194/essd-2026-215, 2026.

Vilgrain, L., Maps, F., Picheral, M., Babin, M., Aubry, C., Irisson, J., and Ayata, S.: Trait-based approach using in situ copepod images reveals contrasting ecological patterns across an Arctic ice melt zone, Limnology and Oceanography, 66, 1155–1167, https://doi.org/10.1002/lno.11672, 2021.

Williams, R., Conway, D. V. P., and Hunt, H. G.: The role of copepods in the planktonic ecosystems of mixed and stratified waters of the European shelf seas, Hydrobiologia, 292, 521–530, https://doi.org/10.1007/BF00229980, 1994.

Zampollo, A., Murray, R. O., Gallego, A., and Scott, B.: Does the oceanographic response to wind farm wind-wakes affect the spring phytoplankton bloom?, Progress in Oceanography, 237, 103 512, https://doi.org/10.1016/j.pocean.2025.103512, 2025.

Zhou, M.: What determines the slope of a plankton biomass spectrum?, Journal of Plankton Research, 28, 437–448, https://doi.org/10.1093/plankt/fbi119, 2006.